Chemical Geology 475 (2017) 76–86

Contents lists available at ScienceDirect

Chemical Geology

journal homepage: www.elsevier.com/locate/chemgeo

Effect of iron and nanolites on Raman spectra of volcanic glasses: A reassessment of existing strategies to estimate the water content

Danilo Di Genova[a,*], Stefania Sicola[b], Claudia Romano[b], Alessandro Vona[b], Sara Fanara[c], Laura Spina[d]

[a] School of Earth Sciences, University of Bristol, Wills Memorial Building, Queens Road, BS8 1RJ Bristol, UK
[b] Dipartimento di Scienze, Università degli Studi Roma Tre, L.go San Leonardo Murialdo 1, 00146 Rome, Italy
[c] Institut für Mineralogie, GZG, Universität Göttingen, Goldschmidtstr. 1, Göttingen, Germany
[d] Department of Physics and Geology, University of Perugia, via Alessandro Pascoli, 06123 Perugia, Italy

ARTICLE INFO

Editor: D.B. Dingwell

Keywords:
Raman spectroscopy
Glasses
Water
Iron
Nanolites

ABSTRACT

The effect of iron content and iron nanolites on Raman spectra of hydrous geologically-relevant glasses is presented. Current procedures to estimate the water content using Raman spectra were tested to explore potential effects of iron content, its oxidation state, and nanolites on models' reliability. A chemical interval spanning from basalt to rhyolite, including alkali- and iron-rich compositions, with water content up to 5.6 wt% was investigated using two spectrometers. When considering nanolite-free samples, the area of the band at 3550 cm^{-1} linearly correlates with the sample water content regardless of chemical composition. Using this approach, data were reproduced with a root-mean-square error (RMSE) of ~0.15 wt%. Depending on the sample chemistry, water content, and acquisition conditions the laser-induced sample oxidation led to underestimating the water content up to ~90% with a long acquisition time (26 min). Normalising the water band region to the silicate band region minimises such a limitation. The area ratio between these bands linearly correlates with the water content and the use of different baseline procedures does not remove the dependence of such a correlation by the iron content and its oxidation state. With this procedure, data were reproduced with a RMSE of ~0.16 wt%. For both approaches, the presence of iron nanolites may result in underestimating the water content.

1. Introduction

Water is the most abundant volatile species dissolved in natural melts and greatly affects, even at low concentration, a variety of thermodynamic and physical properties, from phase equilibria, to reaction kinetics, element diffusivities, electrical conductivity, heat capacity, and partial melting (Behrens and Zhang, 2009; Giordano et al., 2015; Lange and Carmichael, 1990; Poe et al., 2012; Scaillet and Macdonald, 2001; Stebbins et al., 1995). Moreover, bulk properties such as viscosity and density of the melt can vary by several orders of magnitude depending on the dissolved water content (Bouhifd et al., 2015; Dingwell et al., 1996; Lange and Carmichael, 1990; Whittington et al., 2000). Such properties control the entirety of magmatic and volcanic processes occurring from the melt generation, magma rise, decompression and, ultimately, the fate and style of volcanic eruptions.

Volcanic glasses, from glass shards to melt inclusions trapped in crystals, represent the products of most of volcanic eruptions. Analytical studies of water distribution in natural glasses are crucial for understanding the plethora of physical and chemical processes, and their feedbacks, occurring before, during, and after the eruption (Bachmann et al., 2009; Berry et al., 2008; Blundy and Cashman, 2005; Dingwell, 2006; Hartley et al., 2014; Kennedy et al., 2005; Métrich et al., 2010). Moreover, investigations of run products from solubility, diffusion, decompression, crystallisation, and bubble nucleation experiments help to constrain the timescale of physical and chemical processes in hydrous systems (Blundy and Cashman, 2005; Fanara et al., 2015; Gardner et al., 2000; Gonnermann and Gardner, 2013; Hammer et al., 2000; Le Gall and Pichavant, 2016; Martel and Iacono-Marziano, 2015; Shishkina et al., 2010).

Raman spectroscopy is a non-destructive technique used to chemically discriminate glasses, study and estimate the oxygen fugacity and volatile content (e.g., Di Genova et al., 2016a, 2016b; Di Muro et al., 2006a, 2009; Le Losq et al., 2012; Morizet et al., 2013; Thomas, 2000). The minor sample preparation and high-spatial resolution of few μm^2 represent the main advantages of using Raman spectroscopy over other standard techniques typically used for water content determination

* Corresponding author.
E-mail address: danilo.digenova@bristol.ac.uk (D. Di Genova).

https://doi.org/10.1016/j.chemgeo.2017.10.035
Received 25 June 2017; Received in revised form 26 October 2017; Accepted 30 October 2017
Available online 17 November 2017

Table 1
Dry composition (wt%) of the starting materials. The associated errors are reported in Section 2.3 of this work and in the mentioned studies.

Sample	KR[a]	HO[a]	ETN[b]	FR[c]	AMS[b]	PS-GM[b]	472AD[d]	79AD[d]	V_1631_W[e]	RH[f]
Composition	Fe^+ basalt	Dacite	Trachy-basalt	Latite	Trachyte	Fe^+ rhyolite	Fe^+ phonolite	Fe^- phonolite	Tephri-phonolite	Fe^- rhyolite
H_2O[g]	TGA	TGA	KFT + NIR	KFT + NIR	KFT + NIR	KFT + NIR	KFT	KFT	NIR	TGA
SiO_2	50.24	66.17	48.06	56.55	57.72	69.21	51.36	56.09	53.52	78.87
TiO_2	1.99	0.77	1.67	0.81	0.39	0.5	0.48	0.19	0.6	0.10
Al_2O_3	13.55	15.96	16.72	17.92	18.4	9.18	21.63	22.02	19.84	12.52
$FeO_{tot.}$	14.08	5.02	9.92	6.59	4.51	7.94	4.54	2.26	4.8	1.55
MnO	0.25	0.12	0.24	0.17	0.1	0.32	–	–	0.14	0.04
MgO	5.86	1.70	5.46	2.36	1.46	0.08	0.74	0.18	1.76	0.04
CaO	10.09	4.65	10.03	5.52	4.23	0.6	5.90	2.8	6.76	0.84
Na_2O	2.46	3.70	3.68	4.55	3.72	6.52	5.92	6.22	4.66	1.01
K_2O	0.32	2.23	1.83	4.53	7.9	4.35	9.42	10.25	7.91	5.28
P_2O_5	0.55	0.01	0.48	0.01	0.19	0.04	–	–	–	0.02

[a] This study.
[b] Di Genova et al. (2014a).
[c] Di Genova et al. (2014b).
[d] Scaillet and Pichavant (2004).
[e] Romano et al. (2003).
[f] Di Genova et al. (in press).
[g] The dissolved water content in glass was determined by thermogravimetric (TGA), Karl–Fischer titration (KFT), and near-infrared spectroscopy (NIR) analyses.

[Fourier transform infrared spectroscopy (FTIR), Karl Fischer titration (KFT), and thermogravimetric analysis (TGA)]. The potential of Raman spectroscopy, together with progress in the performance of spectrometers, now opens future opportunities for producing high-resolution maps of water distribution in volcanic and experimental products necessary to constrain processes involved in volcanic eruptions and their equilibrium versus disequilibrium timescales.

Over the past few decades, several authors have adopted different protocols for the quantification of water content by Raman spectroscopy based on internal and external calibrations (Behrens et al., 2006; Chabiron et al., 2004; Di Muro et al., 2006b; Mercier et al., 2009; Thomas, 2000; Thomas et al., 2008; Zajacz et al., 2005). The external calibration requires a set of standards where the water content is independently determined (Behrens et al., 2006; Thomas et al., 2008; Mercier et al., 2009). Moreover, each spectrometer needs to be calibrated due to the different performance of detectors and instrumental settings (e.g., grating, excitation source, objective, acquisition time, focus depth) which affect the spectra intensity and the band area. Differently, the internal calibration is based on spectra normalisation between the water and silicate regions. This approach is expected to remove most of instrumental effects on Raman spectra. Therefore, so far, the internal calibration has been considered to allow different laboratories to use a common calibration.

In order to provide a single calibration valid over a large compositional interval, Le Losq et al. (2012) embedded the chemical-dependence of Raman spectra into a background procedure which depends on the sample SiO_2 content (more details are provided in the following sections). After background subtraction, their calibration relied on the ratio (HW/LW) between the water (HW, 2700–3900 cm^{-1}) and silicate (LW, 200–1300 cm^{-1}) area bands to estimate the dissolved water content H_2O (wt%) as follows:

$$\frac{H_2O}{(100 - H_2O)} = A \cdot \frac{HW}{LW} \quad (1)$$

The left member of the equation represents the water/glass proportion and the A coefficient is equal to $7.609 \cdot 10^{-3}$. While A might change with the used spectrometer, the relationship between HW/LW and the water/glass proportion was found to be unique and linear regardless of the sample composition (Le Losq et al., 2012).

However, the starting materials used in their study were mainly iron-free glasses (9 out of 12 glasses). Natural glasses contain iron which is present in both reduced (Fe^{2+}) and oxidised (Fe^{3+}) forms depending on temperature, oxygen fugacity, and chemical composition. The dual behaviour of iron affects the Raman spectra of natural glasses (Di Muro et al., 2009; Di Genova et al., 2016a). Moreover, Di Muro et al. (2006a, 2006b) and Di Genova et al. (in press) found that iron-bearing crystals at the micro- and nanoscale dramatically alter the Raman features of glasses. These particles nucleate and grow during cooling or thermal annealing above the glass transition temperature and have been recently recognised to be pervasive in experimental specimens and natural products (Di Genova et al. in press). Based on these observations, it is evident that any Raman model used to estimate the water content of natural products should consider such effects.

These considerations led us to reassess the relationship between Raman spectra and the water content of volcanic glasses. Here, we investigate a series of hydrous glasses with $FeO_{tot.}$ up to 14.1 wt% characterised by chemical composition spanning from basalt to iron-poor and iron-rich phonolite and rhyolite. We used two Raman instruments to investigate possible effects of diverse instrumental characteristics. This contribution aims to test current strategies and provide reliable procedures to estimate the water content of naturally-occurring glasses by Raman spectrometry.

2. Materials and analytical methods

2.1. Samples from previous studies and starting materials

To explore chemical effects on Raman spectra of glasses, we investigated hydrous samples with variable water content over a wide range of chemical composition. Sample set includes 20 glasses from previous studies and 9 glasses synthesised specifically for this study. In term of silica, iron, and alkali content, the used compositions span almost the entire chemical spectrum of magmas erupted on Earth.

2.2. Samples and starting material from previous studies

The chemical composition of samples synthesised in previous studies is reported in Table 1 and shown in a TAS (total alkali versus silica) diagram in Fig. 1A. The samples include:

- Trachybasalt (ETN, Di Genova et al., 2014a) from Etna (1991–1993 lava flow field in Val Calanna, Italy);
- Latite (FR, Di Genova et al., 2014b) from Fondo Riccio eruption (9.5 ka Campi Flegrei, Italy);

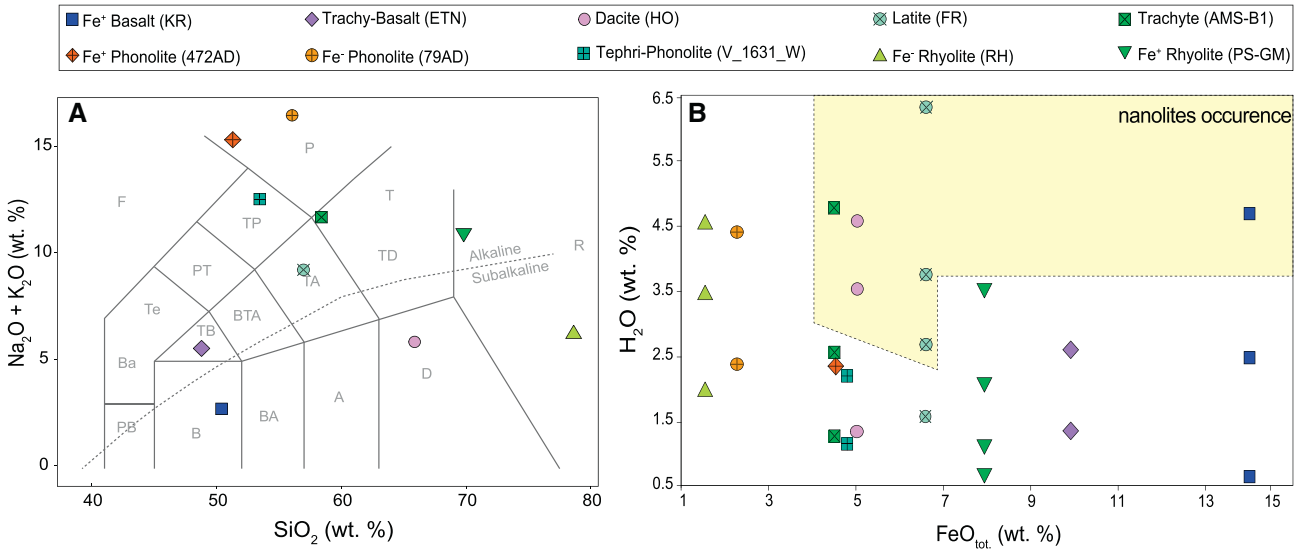

Fig. 1. A) TAS (total alkali versus silica) diagram showing the composition of samples used in this work. KR and HO glasses were synthesised in this study, while all other glasses were previously synthesised (see Table 1 for samples reference). Abbreviations in the plot mean: PB - picrobasalt, B - basalt, BA - basaltic andesite, A - andesite, D - dacite, R - rhyolite, TB - trachybasalt, BTA - basaltic trachyandesite, TA - trachyandesite, TD - trachydacite, T - trachyte, Ba - basanite, Te - tephrite, PT - phonotephrite, TP - tephriphonolite, P - phonolite, F - foidite. B) Samples water content (wt%) as a function of $FeO_{tot.}$ (wt%). The shaded area shows the occurrence of iron-bearing nanolites in some of the investigated samples (see text for a detailed discussion). The sample water content is reported in Table 2.

- Trachyte (AMS-B1, Di Genova et al., 2014a) from Agnano Monte Spina eruption (4400 BP Campi Flegrei, Italy);
- Phono-tephrite (V_1631_W, Romano et al., 2003) from AD 1631 Vesuvius eruption;
- Tephri-phonolite (472AD) and phonolite (79AD) from Scaillet and Pichavant (2004) belonging to the main explosive phases of Pollena (472AD) and Pompei (79AD) Vesuvius eruptions;
- Iron-rich rhyolite (PS-GM, Di Genova et al., 2013) from the Khaggiar lava flow (8.2 to 5.5 ka Pantelleria, Italy);
- An anhydrous iron poor-rhyolite (RH, Di Genova et al. in press) with chemistry similar to rhyolitic melts of the Yellowstone Plateau Volcanic Field (USA).

Details of the experimental procedures employed to synthesise hydrous glasses are reported in the mentioned studies. Detailed anhydrous composition and water contents (determined by FTIR, TGA, and/or KFT) are reported below.

2.3. Samples synthesised in this study

In addition to the samples from literature, two anhydrous glasses belonging to the calcalkaline magma series were produced starting from: i) a basalt (KR) from the 1984 lava flow at Krafla volcano (Iceland; Tryggvason, 1986); ii) a dacite (HO) from AD 1707 Hoei eruption at Mt. Fuji (Japan; Miyaji et al., 2011).

The rocks were melted in a thin-walled Pt crucible using a Nabertherm $MoSi_2$ box furnace at 1400 °C for 5 h and rapidly quenched in air. Glass chips from KR and HO samples were separately loaded into a $Pt_{80}Rh_{20}$ crucible. A concentric cylinder assembly was used to chemically homogenise the samples and remove bubbles from the melts. Samples were continuously stirred at 1 atm from 4 h to 1 day at 1400 °C until the melt was free of bubbles and completely homogenised. Afterwards, the sample was rapidly quenched by immerging the crucible in water. The obtained glasses were chemically characterised and prepared for hydrous synthesis.

Chemical compositions were measured with a Cameca SX100 electron micro probe analyser (EMPA) using a defocused beam (10-μm) to minimise alkali loss. Analyses were carried out at 15 kV acceleration voltage and 5 nA beam current. Wollastonite (Ca, Si), periclase (Mg), hematite (Fe), corundum (Al), natural orthoclase (K), and albite (Na) were used as standards. Additionally, a matrix correction was performed according to Pouchou and Pichoir (1991). The precision was better than 2.5% for all analysed elements. The chemical homogeneity of glasses was verified by performing ~25 chemical analyses for each sample.

In order to obtain water-bearing glasses, anhydrous glasses from KR and HO, together with the iron-poor rhyolite RH (Di Genova et al. in press), were powdered and sieved to obtain two powder fractions with grain sizes of 200–500 μm and < 200 μm. Afterwards, powders were loaded into AuPd capsules (3 mm outer diameter, 10 mm lengths, 0.2 mm wall thickness) with a weight ratio of 1:1 to minimise the pore volume together with the appropriate amount of doubly distilled water. Syntheses were performed at 260 MPa and at 1250 °C for 3 days in an internally heated gas pressure vessel (IHPV) at the Institute of Mineralogy at the University of Göttingen using the drop-fast quench technique. Samples were placed in the furnace hot zone through a platinum wire. At the end of the experiment, the wire was melted with a sudden D.C. current and samples were quenched rapidly in the cold part of the vessel. Each capsule was weighted before and after the experiment to test for possible leakage. The obtained glasses were free of bubbles and crystals at the microscale. Each composition was nominally hydrated with three different water contents of ~1, ~3, and ~4.5 wt%.

Dissolved water content in glasses was measured using the Fourier Transform Infrared (FTIR) spectroscopy technique and thermogravimetric analysis (TGA). We used a Bruker Vertex 70 spectrometer coupled with an IR Microscope Hyperion 3000 at the Institute of Mineralogy at the University of Göttingen. For NIR analyses, each sample was double-polished below ~400 μm thickness measured using a Mitutoyo instrument (error of 2 μm). The densities of the water-bearing glasses were calculated after Lange and Carmichael (1987). The Lambert-Beer law was used to determine the sample water content (Stolper, 1982) using the NIR and MIR spectra (see the Supplementary materials section and Table S1 for measurements details).

Thermogravimetric analyses were performed using a Setaram™ TGA 92 instrument at the Institute of Mineralogy at the University of Göttingen. Between 10 and 20 mg of coarsely powdered glass was loaded into a Pt crucible (4 mm diameter, 10 mm height) covered with a Pt lid. The sample was heated from ambient temperature at 10 °C/min

up to 1200 °C. After a dwell time of 30 min, the sample was cooled at 30 °C/min to room temperature. During the entire analysis, the sample weight loss was continuously recorded. To account for buoyancy changes with temperature of the sample and therefore correct the measured sample weight loss, a subsequent heating and cooling cycle was performed with the degassed sample (Schmidt and Behrens, 2008). For each sample, three thermogravimetric analyses were performed.

2.4. Raman spectroscopy

Raman spectra were acquired with two different Raman instruments available at the Mineralogical State Collection of Munich (SNSB, Horiba XploRa-Raman-System) and Department of Science at Roma Tre University (Horiba LabRam HR 800) hereafter termed M and R spectrometers, respectively. For each sample, 10 spectra were acquired to investigate the experimental reproducibly of the results.

The instruments are equipped with an attenuated doubled Nd3:YAG laser having a wavelength of 532 nm and a microscope. The laser power on the sample surface was measured to be 7.15 mW (M spectrometer) and 11 mW (R spectrometer) through a 100 × objective and ~5 μm^2 spot size. The instruments were calibrated using a silicon standard. Instrumental settings consisted of 1800 grooves/mm grating density, confocal hole of 300 μm and slit of 200 μm with an exposure time of 60 s (3 times). The backscattered Raman radiation was collected on a polished sample surface over a range from 100 to 1500 cm^{-1} and from 2700 to 4000 cm^{-1} hereafter defined as the low-wavenumber (LW) and high-wavenumber (HW) regions respectively. In total, the M spectrometer required 6 min to acquire both LW and HW regions, while for the R spectrometer 26 min were necessary. Raman signal was found to be maximised at 6 μm of depth using a motor on the Z axis. Therefore, spectra were collected at the same depth for all samples. Prior the Raman spectra acquisition, the samples were stored at 100 °C in an oven to avoid water absorption on the surface.

3. Raman spectra treatment

Raman spectra intensity were corrected for the frequency-dependence scattering intensity and temperature (Long, 1977; Neuville and Mysen, 1996) as it follows:

$$I = I_{obs} \cdot \left\{ \nu_0^3 \cdot \nu \frac{[1 - \exp(-hc\nu/kT)]}{(\nu_0 - \nu)^4} \right\} \quad (2)$$

where I_{obs} is the Raman spectra intensity, ν_0 is the wavenumber of the incident laser light (10^7/532 cm^{-1} for the green laser), ν is the measured wavenumber in cm^{-1}, h is the Planck constant (6.62607 × 10^{-34} J s), c is the speed of light (2.9979 × 10^{10} cm s^{-1}), k is the Boltzmann constant (1.38065 × 10^{-23} J K^{-1}) and T the absolute temperature.

Several procedures have been proposed to remove the spectra background (e.g., Behrens et al., 2006; Le Losq et al., 2012) with the aim to provide a general and chemically independent model to estimate the water content. Here, Matlab© and R codes were developed to fully automatize the background subtraction procedure (see Supplementary materials for the Matlab© code). We followed two different approaches to determine the spectra background in the LW region: the SiO_2-dependent procedure provided by Le Losq et al. (2012) and a compositionally independent strategy (this study).

The background subtraction procedure from Le Losq et al. (2012) relies on the definition of a set of zones devoid of peaks (Background Interpolation Regions, BIRs) to constrain the baseline. Specifically, in the silicate region (100–1500 cm^{-1}, LW), the number and wavelength interval of BIRs depend on the SiO_2 content, while in the water region (2700–4000 cm^{-1}, HW) two BIRs are maintained constant regardless of the composition. The results showed that the independently measured water content correlates linearly with the ratio between the LW and the HW band areas. In this work, we explored the possibility to extend this strategy to a wide range of naturally-occurring iron-bearing glasses with different iron oxidation state. Furthermore, we tested a baseline subtraction procedure based on a single cubic spline fitting independent on the chemical composition (Di Genova et al., 2015). With this, we aim to provide a simple and reproducible procedure to estimate the baseline of iron-bearing glasses which are characterised by a substantial spectral variability and fluorescence (see Results section) due to the effect of the iron content, its oxidation state, and the presence of iron-bearing nanolites on Raman spectra. This would help when analysing samples with unknown chemical composition, namely small melt inclusions trapped in crystals. By using Raman spectra, this study provides best procedures to both estimate water content of natural glasses and recognize iron nanolites.

4. Results

The measured chemical compositions of anhydrous glasses from this study (KR, HO) and samples from previous studies are listed in Table 1. Samples are also shown in a TAS diagram (Fig. 1A). Overall, SiO_2 content spans from ~48 to ~79 wt%, with Na_2O + K_2O between ~2.8 and ~16.5 wt%, $FeO_{tot.}$ and H_2O up to ~14 and 4.53 wt%, respectively (Fig. 1B).

The Table S1 shows the water content measured by FTIR for samples synthesised in this study, while in Table 2 the TGA results obtained from the same samples. Furthermore, estimations from previous studies are reported for the other samples are listed.

For the iron-poor rhyolite (RH) and dacite (HO), the water content was estimated using the peak intensity of the 4500 and 5200 cm^{-1} (Table S1, Fig. S1A, B) attributed to the combination of stretching and bending of OH groups bonded to tetrahedral cations and to the combination of stretching and bending modes of H_2O molecules, respectively. A linear baseline was applied to the RH and OH spectra (Fig. S1A). For the RH and HO samples, we used the linear molar adsorption coefficients given by Ohlhorst et al. (2001) and Withers and Behrens (1999), respectively (details are reported in the Supplementary materials section).

The KR basalt was opaque at thickness compatible with the analyses in the NIR range due to its high iron content (12.79 wt%) which hindered the water quantification. The KR spectra displayed a broad band at ~5700 cm^{-1} which is attributed to crystal field transitions of iron (Ohlhorst et al., 2001) and, possibly, to the presence of iron-bearing nanolites. Therefore, for this composition, we used the band at 3550 cm^{-1} (MIR) to determine the amount of dissolved water in glasses. A linear baseline was applied to evaluate the peak height together with the adsorption coefficient given by Stolper (1982) (Supplementary materials and Fig. S1B).

Concerning the TGA analysis of hydrous samples, it must be noted that for the iron-rich samples such as the KR series, the H_2O content may be underestimated due to the iron oxidation during the high-temperature extraction of water by releasing H_2 instead of H_2O. Assuming initial extremely reduced conditions and, therefore, the iron only existing in a reduced state (Fe^{2+}), we calculated that the water concentration would be underestimated to a maximum of 0.8 wt% for the KR3 sample (H_2O = 4.67 wt%). However, the IHPV used for the sample hydration is about 3 log units above the Ni-NiO buffer and a significant fraction of Fe^{3+} is expected. Therefore, we estimated that the water content may be underestimated to a maximum of ~0.25 wt% (see Schmidt and Behrens, 2008 for a detailed discussion).

The estimated water content for RH, HO, and KR samples using FTIR and TGA agrees within ~10% (Tables 2 and S1 for TGA and FTIR results, respectively). In the following, we consider the water content estimated via TGA.

Table 2
Measured and estimated samples water content of nanolite-free samples (chemical composition in Table 1). For both spectrometers (M and R), the calculated *HW/LW* ratio, *m* coefficient (Eq. (4)) and estimated water contents are reported.

Sample	Composition	H_2O (wt%)	M spectrometer						R spectrometer				
			HW/LW[a]	std. dev.	H_2O[b]	*m*[c]	H_2O[d]	H_2O[e]	*HW/LW*[a]	std. dev.	*m*[c]	H_2O[d]	H_2O[e]
KR1	Fe^+ basalt	0.6 ± 0.04	0.33	0.02	0.68	2.04	0.68	0.67	0.38	0.05	1.83	0.69	0.76
KR2[g]	Fe^+ basalt	2.44 ± 0.06	1.19	0.02	–	2.04	2.42	2.40	1.32	0.06	1.83	2.42	2.66
KR3[f]	Fe^+ basalt	4.67 ± 0.07	1.88	0.02	–	–	–	–	1.43	0.09	–	–	–
HO1[g]	Dacite	1.36 ± 0.06	0.97	0.04	–	1.40	1.36	1.12	0.95	0.04	1.44	1.36	1.08
HO2[f]	Dacite	3.54 ± 0.06	2.79	0.11	–	–	–	–	2.24	0.05	–	–	–
HO3[f]	Dacite	4.58 ± 0.08	3.82	0.14	–	–	–	–	3.10	0.11	–	–	–
RH1	Fe^- rhyolite	1.97 ± 0.03	3.20	0.13	1.76	0.66	2.11	2.60	2.54	0.07	0.72	1.84	2.07
RH2	Fe^- rhyolite	3.45 ± 0.06	5.04	0.12	3.21	0.66	3.32	4.09	4.67	0.05	0.72	3.38	3.79
RH3	Fe^- rhyolite	4.53 ± 0.05	6.91	0.20	4.73	0.66	4.56	5.61	6.40	0.04	0.72	4.63	5.20
ETN1	Trachy-basalt	1.37 ± 0.05	0.88	0.02	1.28	1.78	1.57	1.43	0.88	0.02	1.63	1.44	1.42
ETN2[g]	Trachy-basalt	2.61 ± 0.04	1.39	0.06	–	1.78	2.48	2.25	1.57	0.07	1.63	2.57	2.55
LAT1[g]	Latite	1.59 ± 0.05	1.05	0.03	–	1.51	1.59	1.37	–	–	–	–	–
LAT2[f]	Latite	2.69 ± 0.05	1.43	0.04	–	–	–	–	–	–	–	–	–
LAT3[f]	Latite	3.76 ± 0.04	2.46	0.10	–	–	–	–	–	–	–	–	–
LAT4[f]	Latite	6.32 ± 0.08	7.34	0.95	–	–	–	–	–	–	–	–	–
AMS1	Trachyte	1.29 ± 0.08	1.41	0.09	1.40	0.90	1.27	1.55	1.23	0.02	1.02	1.26	1.35
AMS2	Trachyte	2.57 ± 0.10	2.85	0.10	2.46	0.90	2.58	3.13	2.52	0.06	1.02	2.58	2.77
AMS3[f]	Trachyte	4.78 ± 0.09	3.63	0.04	–	–	–	–	–	–	–	–	–
PS-GM0.5	Fe^+ rhyolite	0.72 ± 0.04	0.74	0.02	0.77	1.32	0.98	1.06	0.62	0.03	1.38	0.85	0.88
PS-GM1	Fe^+ rhyolite	1.16 ± 0.02	1.08	0.01	1.18	1.32	1.43	1.55	0.92	0.01	1.38	1.27	1.31
PS-GM2	Fe^+ rhyolite	2.11 ± 0.05	1.70	0.02	1.96	1.32	2.24	2.43	1.48	0.02	1.38	2.03	2.11
PS-GM3.5[g]	Fe^+ rhyolite	3.55 ± 0.04	2.48	0.06	–	1.32	3.27	3.54	2.56	0.05	1.38	3.53	3.65
V_1631_1	Tephri-fonolite	1.17 ± 0.05	1.58	0.02	1.50	1.00	1.59	1.78	1.29	0.07	1.22	1.57	1.45
V_1631_2	Tephri-fonolite	3.07 ± 0.12	2.90	0.04	3.10	1.00	2.91	3.26	2.41	0.16	1.22	2.94	2.71
V_1631_3[g]	Tephri-fonolite	3.32 ± 0.13	3.24	0.04	–	1.00	3.26	3.58	2.63	0.10	1.22	3.21	2.96
79AD1	Fe^- phonolite	2.39	–	–	–	–	–	–	2.11	0.07	0.96	2.03	1.85
79AD2	Fe^- phonolite	4.41	–	–	–	–	–	–	4.74	0.06	0.96	4.57	4.18
472AD1	Fe^+ phonolite	2.36	–	–	–	–	–	–	2.47	0.04	0.96	2.36	2.72
External sample	Trachyte	5.57	6.08	0.18	5.58	0.90	5.49	6.42	–	–	–	–	–

[a] Calculated area ratio between the water (HW) and silicate (LW) bands.
[b] Calculated water content using the HW band area and Eq. (3).
[c] Calculated linear coefficient *m* (Eq. (4)).
[d] Calculated water content using the HW/LW ratio and Eq. (4).
[e] Calculated water content using the $FeO_{tot.}$ (wt%) and Eqs. (4) and (5).
[f] Nanolite-bearing samples.
[g] Sample alteration due to laser-induced heating (M spectrometer conditions, see Discussion section for details).

5. Discussion

5.1. Effect of the chemical composition, water content, and iron nanolites on Raman spectra

Fig. 2 shows the LW region of a selection of corrected (Eq. (2)) spectra from anhydrous glasses to highlight differences in Raman features due to the composition. Spectra with a different SiO_2 content were vertically superimposed and listed by increasing iron content from the bottom. The most striking difference between spectra can be observed in the region around 1000 cm^{-1}. The iron-poor rhyolite (RH) exhibits the lowest signal to background ratio. At higher iron content, the signal to background ratio substantially increases. Moreover, excluding the iron-poor rhyolite (RH), all samples show a clear contribution at ~970 cm^{-1} in accordance with previous studies performed on iron-bearing multicomponent systems (Di Genova et al., 2015; Di Muro et al., 2009).

The region below 700 cm^{-1} (Fig. 2) is attributed to T–O–T angle bending/rocking vibrations and tetrahedral O–Si–O bending vibrations (McMillan, 1984; Mysen et al., 1982). The broad band centred at ~500 cm^{-1} represents vibrational motions involving bridging oxygens associated with a wide range of T–O–T environments. This region originates from rings of tetrahedra connected in three-, four-, five-, six- or higher-members (Bell et al., 1968; Galeener, 1982; McMillan, 1984; Mysen et al., 1982; Poe et al., 2001; Seifert et al., 1982; Sharma et al., 1981). The region between 800 and 1300 cm^{-1} results from T–O stretching vibrations and provides information on the distribution of bridging oxygens and therewith on the degree of polymerization of the structure (Bell and Dean, 1972; Furukawa et al., 1981; McMillan, 1984; Mysen, 2003). Moreover, recent studies (Di Genova et al., 2017; Di Muro et al., 2009) drew the attention to the effect of iron redox state on this region for anhydrous rhyolitic glasses. These studies reported direct

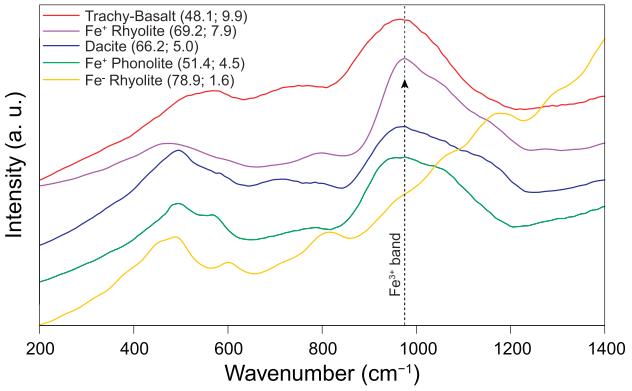

Fig. 2. Raman spectra (LW region) of anhydrous glasses corrected for the excitation line and temperature (Eq. (2)) and normalised to the total area. Spectra were listed with increasing iron content from the bottom. The signal-background ratio is extremely low for the iron-poor rhyolite (RH). All the other spectra show higher signal-background ratio and a contribution at ~970 cm^{-1} (Fe^{3+} band). Fe^+ and Fe^- in the legend indicate iron-rich and iron-poor compositions in Table 1, while numbers show the SiO_2 and iron content in wt%, respectively.

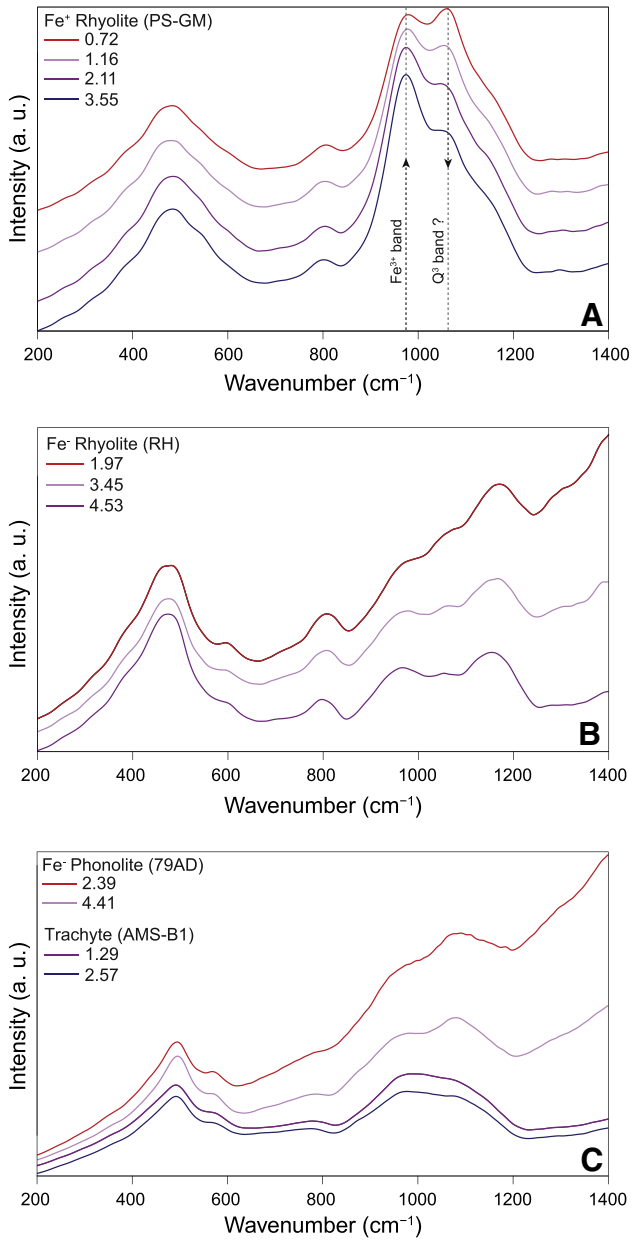

Fig. 3. A) Corrected Raman spectra (LW region) of iron-rich rhyolitic series (PS-GM, SiO_2 = 69.21 wt% and $FeO_{tot.}$ = 7.94 wt%). With increasing water content, the Fe^{3+} band increases due to the increase of $Fe^{3+}/Fe_{tot.}$ ratio measured by Di Genova et al. (2013). Simultaneously, the band at 1060 cm^{-1} decreases possibly due to the structure depolymerisation (see text for discussion). Numbers in the legend show the dissolved water content in wt%. B) Corrected Raman spectra (LW region) of iron-poor rhyolitic series (RH, SiO_2 = 78.87 wt% and $FeO_{tot.}$ = 1.55 wt%). The spectra background decreases with increasing water content. Numbers in the legend show the dissolved water content in wt%. C) Corrected Raman spectra (LW region) of samples with ~57 wt% SiO_2 content. The iron-poor phonolite (79AD, $FeO_{tot.}$ = 2.26 wt%) shows a different spectra background depending on the dissolved water content (as observed in Fig. 5B). The trachyte, higher in $FeO_{tot.}$ content (4.51 wt%), shows a constant spectra background (as observed in panel A for the Fe^{+} rhyolite). Numbers in the legend show the dissolved water content in wt%.

correlations between the intensity of the band at 970 cm^{-1} with the $Fe^{3+}/Fe_{tot.}$ ratio of the glass. Di Genova et al. (2017) showed that such a contribution 1) increased with the structure polymerization of the anhydrous glass and 2) disappeared in Raman spectra of iron-free rhyolites. Moreover, based on XANES spectra, Stabile et al. (2017) suggested that the Fe^{3+} is four-fold coordinated in these systems. According to these recent results, Di Genova et al. (2017) named the ~970 cm^{-1} contribution of Raman spectra of rhyolites as "Fe^{3+} band".

Here, looking at the hydrous iron-rich rhyolite spectra (Fe^{+} rhyolite, PS-GM series, $FeO_{tot.}$ = 7.94 wt%, Fig. 3A), for which the $Fe^{3+}/Fe_{tot.}$ ratio is known (Di Genova et al., 2013), we observe that the Fe^{3+} band increases with increasing $Fe^{3+}/Fe_{tot.}$ ratio from 0.36 (PS-GM0.5, H_2O = 0.72 wt%) to 0.56 (PS-GM3.5, H_2O = 3.55 wt%). This agrees with previous observations from anhydrous samples (Di Genova et al., 2017; Di Muro et al., 2009).

Furthermore, with increasing water content, the spectral contribution at 1060 cm^{-1} clearly decreases. This band may be assigned to symmetric stretching of tetrahedra with 3 bridging oxygens (Q^3 species, Mysen et al., 1980; Zotov and Keppler, 1998). Therefore, for these samples, we suggest that the decrease of this band is directly related to the increase of water content depolymerising the silicate structure (Zotov and Keppler, 1998). This would explain the measured decrease in viscosity (Di Genova et al., 2013) and glass transition temperature (Di Genova et al., 2014a) upon hydration for these samples although the oxidation state of the system increases with water and, therefore, an opposite behaviour would be expected (Di Genova et al., 2017). However, in a multicomponent glass, the spectral contributions are not well-resolved, and a systematic study based on spectra deconvolution is required to carefully address this aspect.

Raman spectra of the iron-poor rhyolite (Fe^{-} rhyolite, RH series, $FeO_{tot.}$ = 1.55 wt%, Fig. 3B) show a different behaviour. Spectra are characterised by a high fluorescence which decreases with increasing water content.

To obtain a clear picture of the combined effect of iron and water on Raman features of glasses with different chemical compositions, a comparison between samples with lower SiO_2 content (~57 wt%) is reported in Fig. 3C. Spectra from the phonolite (79AD) and trachyte (AMS-B1) with iron respectively equal to 2.26 and 4.51 wt% were used. As observed for the Fe^{-} rhyolite (Fig. 3B), the iron-poor samples (Fe^{-} phonolite, 79AD series) display a background which changes with water content. Conversely, the iron-rich spectra (trachyte, AMS-B1 series) are characterised by a constant background as showed before for the iron Fe^{+} rhyolite (Fig. 3A). Therefore, the amount of iron and its oxidation state (modulated by the water content) play a role in defining the variability of the spectra fluorescence of volcanic glasses.

With increasing iron content (> 4.5 wt%) we observed a substantial variation in the Raman features. In Fig. 4A, B the LW and HW regions of dacitic spectra (HO series) are reported, respectively. With increasing water content (≥ 3.54 wt%), the spectra show three main features: 1) the lowering of the silicate (LW) region area, 2) the development of a peak at ~690 cm^{-1} (Fig. 4A) and 3) no changes of the water band (HW) with water content (Fig. 4B).

Analogous spectral signature was acknowledged by Di Muro et al. (2006a, 2006b) and Di Genova et al. (in press) for dacitic, trachytic and rhyolitic samples. Di Genova et al. (in press) experimentally demonstrated that both the quench from *liquidus* condition and the heating above the glass transition temperature induced the crystallisation of iron oxides at the nanoscale. Here, the nanolite occurrence seems to be related to the high element diffusivity due to the extremely low-viscosity of hydrous melts at *liquidus* condition. Indeed, excluding the relatively viscous iron-rich rhyolite (PS-GM, see Di Genova et al., 2013 for viscosity measurements and comparisons with other compositions), samples with $FeO_{tot.}$ and H_2O respectively higher than ~4.5 and ~3 wt% crystallised nanolites.

Importantly, nanolites were present in our samples before the Raman measurements and were not detected during microprobe analyses. Therefore, we can exclude their occurrence induced by the laser heating of glasses. To confirm that, we performed high resolution SEM analyses on pristine samples that revealed the presence of whitish particles at the nanoscale (Fig. S2). This is in line with results reported by Di Genova et al. (in press). There, magnetic-hysteresis analyses were performed on nanolite-bearing samples. Magnetite nanolites with diameters between ~5 nm to ~30 nm were detected. Therefore, our

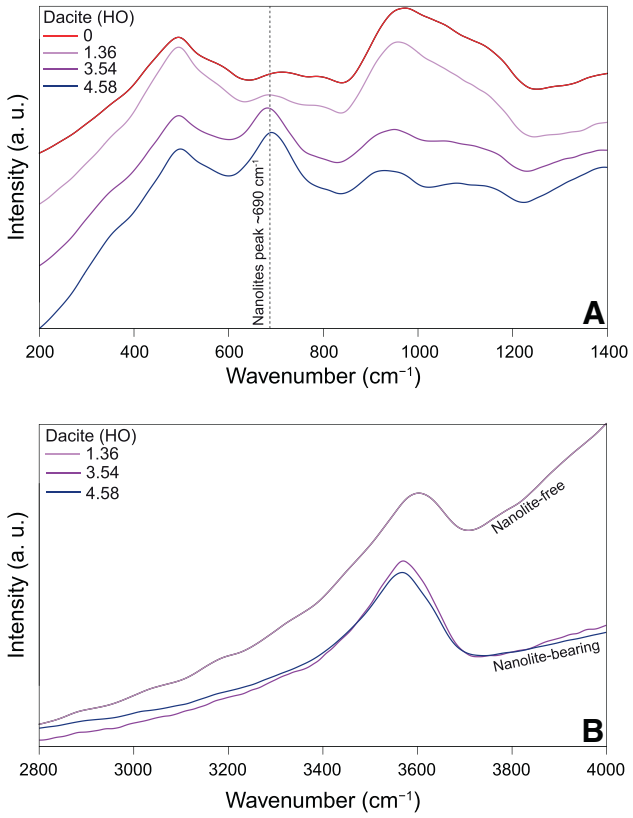

Fig. 4. A) Corrected Raman spectra (LW region) of the dacitic series (HO, $FeO_{tot.}$ = 5.02 wt%). With increasing water content, spectra show a peak at ~690 cm^{-1} due to the iron-bearing nanolites occurrence. Numbers in the legend show the dissolved water content in wt%. B) Corrected Raman spectra (HW region) of the dacitic series (HO, $FeO_{tot.}$ = 5.02 wt%). Nanolite-bearing samples, characterised by a different water content (H_2O = 3.54 and 4.58 wt%), exhibit a similar band area. Numbers in the legend show the dissolved water content in wt%.

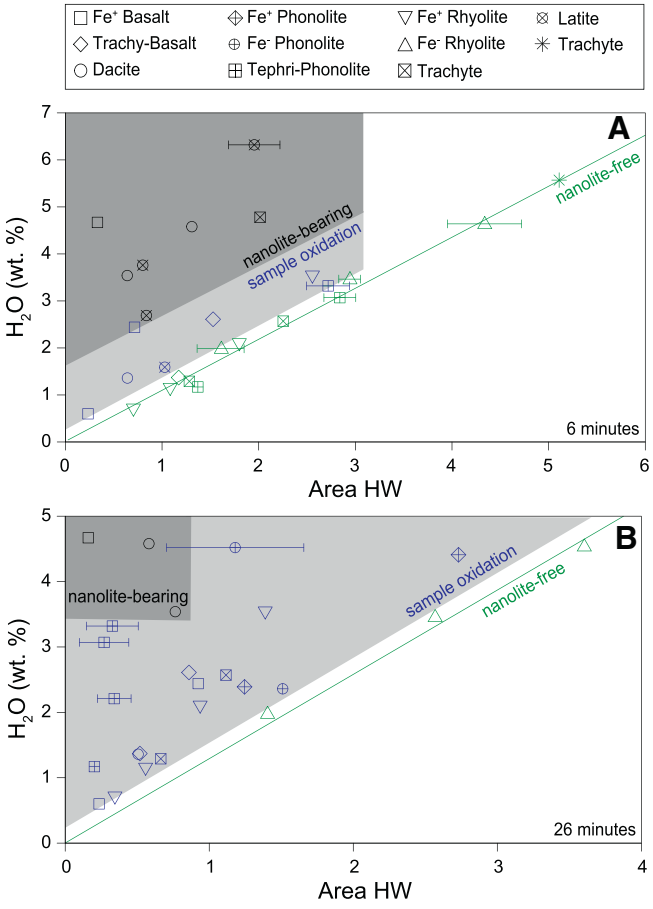

Fig. 5. Area of the HW band for samples investigated in this study. Samples distribute in 3 different regions identified by sample colours: green symbols indicate nanolite-free samples, blue symbols represent nanolite-free samples that experienced surface oxidation during the analysis (light-grey area), while black symbols represent nanolite-bearing samples (dark-grey area). A linear relationship between the sample water content and HW area can be observed for nanolite-free samples which did not experience surface oxidation due to the acquisition timescale (see text for a detailed discussion). All nanolite-bearing samples deviate from the linear relationship. Band area has been divided by 10^5. A) Data from M spectrometer, total acquisition time 6 min (3 min for the LW region and 3 min for the HW region). The trachyte (* symbol, H_2O = 5.57 wt% external sample in Table 2) was used to validate the calibration. B) Data from R spectrometer (total acquisition time 26 min). Some samples were not measured with both spectrometers (see Table 2). (For interpretation of the references to colour in this figure legend, the reader is referred to the web version of this article.)

results demonstrate that Raman spectroscopy can also be used to show the presence of iron-bearing nanolites in volcanic glasses. This will help to reveal overlooked features in the glass matrix of experimental syntheses and natural rocks. Moreover, the presence of nuclei at the nanoscale can affect the onset of (heterogeneous) crystallisation of other phases and degassing of volatiles during cooling and/or decompression and, ultimately, the magma rheology (Di Genova et al. in press). Based on the documented effect of the chemical composition, oxygen fugacity and iron nanolites on Raman spectra, we reassessed the current methodologies to estimate the water content dissolved in volcanic glasses.

5.2. Quantification of the dissolved water content

5.2.1. Water content versus HW band area

The effect of increasing H_2O content on the HW band for nanolite-free and nanolite-bearing samples is shown in Fig. 5A, B for both spectrometers. For nanolite-free samples (green symbols), the HW area band linearly increases with increasing water content. Therefore, for a single spectrometer, a (set of) glass standard(s) is sufficient to estimate the water content of unknown samples with different chemical composition. Importantly, spectra must be collected using the same experimental settings (see Materials and analytical methods section).

However, for some nanolite-free samples, a deviation from linearity was observed (Fig. 5A, B). Looking at results from the M spectrometer (blue symbols, bright-grey area in Fig. 5A), where spectra were acquired in 6 min (LW + HW region), the iron-rich samples (KR and ETN basalts, FR latite and the PS-GM iron-rich rhyolite sample with maximum water content) exhibit a HW area lower than expected. Concerning the data from the R spectrometer (Fig. 5B), and except for the iron-poor rhyolitic series (RH), all the nanolite-free samples deviate from the linearity. The time necessary to acquire a single spectrum (LW + HW region) using the R spectrometer was 26 min, four times longer than the time needed when using the M spectrometer. For these spectra, we clearly observed a change in the LW region. In fact, when comparing the spectra normalised to the region related to the T—O—T environment (~500 cm^{-1}), we observed that the spectra intensity increased at ~970 cm^{-1} (i.e. the Fe^{3+} band increased, Fig. S3). Furthermore, the intensity increased with the acquisition time suggesting that the laser heating induced the oxidation of the glass. We noted that this was particularly relevant for alkali-rich composition such as the tephri-phonolite (Fig. S3). We explain the observed decrease of the HW area (Fig. 5A and B) with the degassing of dissolved H_2O through iron oxidation according to the following reaction: $H_2O + 2FeO = H_2 + Fe_2O_3$ (Burgisser and Scaillet, 2007; Humphreys et al., 2015).

In order to avoid the sample oxidation and provide the best experimental conditions to estimate the water content, we performed

several tests varying the laser power and/or the spectra acquisition time. By combining the results obtained from both spectrometers, we recommend a laser power of ≤ 5 mW on the sample surface and acquisition time of 5 min maximum (using the 100 × objective). For silica-poor and iron-rich hydrous (nanolite-free) systems (basalt, latite and, at lesser extent, Fe-rich rhyolite), the sample surface may oxidise within 6 min using a laser power of 7.15 mW on the sample surface. The sample oxidation results in the underestimation of the sample water content using the calibration based on the HW band area (i.e. external calibration). Increasing the acquisition time and laser power (up to 26 min and 11 mW) this effect occurs regardless of the glass composition with the exception of the iron-poor rhyolite (RH).

Nanolite-bearing samples differently deviate from the linear relationship observed in Fig. 5A, B depending on the sample composition. The HW area of nanolites-bearing samples is lower than expected for a given water content (Fig. 4B). This might be related to a decrease in the analysed hydrous glass volume due to the presence of nanolites. However, since the effect of nanolites on the water estimation using standard techniques is unknown, more studies are required to investigate their effect on KFT, TGA and NIR analyses.

Therefore, the estimation of the sample water content based on the comparison of the HW band area (Fig. 5A, B) must be used only for nanolite-free samples where sample oxidation did not occur. For the M spectrometer, we derived the linear relationship between the HW and the water content as it follows:

$$H_2O\ (wt\%) = 1.\ 092{\cdot}10^{-5}{\cdot}HW \quad (3)$$

where HW represents the water band area of Long-corrected spectra (Eq. (2)). It must be noted that this relationship is valid for the M spectrometer using the experimental conditions reported in Section 2.4. We recommend that laboratories develop a specific calibration applicable to their instrument, measuring condition and spectra treatment procedure.

A spectrum from a trachyte with H_2O = 5.57 wt% estimated by KFT ("external sample" Table 2) was acquired. Using the Eq. (3), we estimated the water content equal to 5.58 wt%. Therefore, over a large interval of composition, a linear relationship between the HW band area and the water content can be used to estimate the water content provided that the sample surface does not oxidise during the spectra acquisition.

5.2.2. Water content versus HW/LW band area ratio

For a given sample, the HW/LW band ratio depends on the procedure employed for background subtraction in the LW region. Fig. 6A, B, C show the background subtraction procedure following Le Losq et al. (2012) and the protocol used in this study. Nanolite-bearing samples were not compared as the intermediate Raman region (640–740 cm^{-1}) is heavily affected by the spectral signature of nanolites (Fig. 4A) and, therefore, the background could not be assessed following the Le Losq et al. (2012) model.

While for SiO_2-rich systems (Fig. 6A, B) both procedures returned similar results, for SiO_2-poor systems (Fig. 6C) the baseline strategies resulted in different spectra and, therefore, different LW areas for the same sample. This agrees with that reported by Le Losq et al. (2012). We estimated the dissolved water content of our glasses using the Le Losq et al. (2012) model. The measured water contents versus model predictions are given in Fig. 7. The RMSE of the model prediction is 0.68 wt% which decreases to 0.32 wt% if only samples with water content below 2 wt% are considered. At H_2O > 2 wt%, the model overestimates and underestimate the measured data for iron-poor and iron-rich samples, respectively.

These results suggest that the *A* coefficient from Eq. (1) depends on the composition, especially on iron content. Our findings suggest that, although removing some of the chemical dependence (from SiO_2), the background procedure proposed by Le Losq et al. (2012) does not completely account for the composition of glasses with variable iron content and oxidation state.

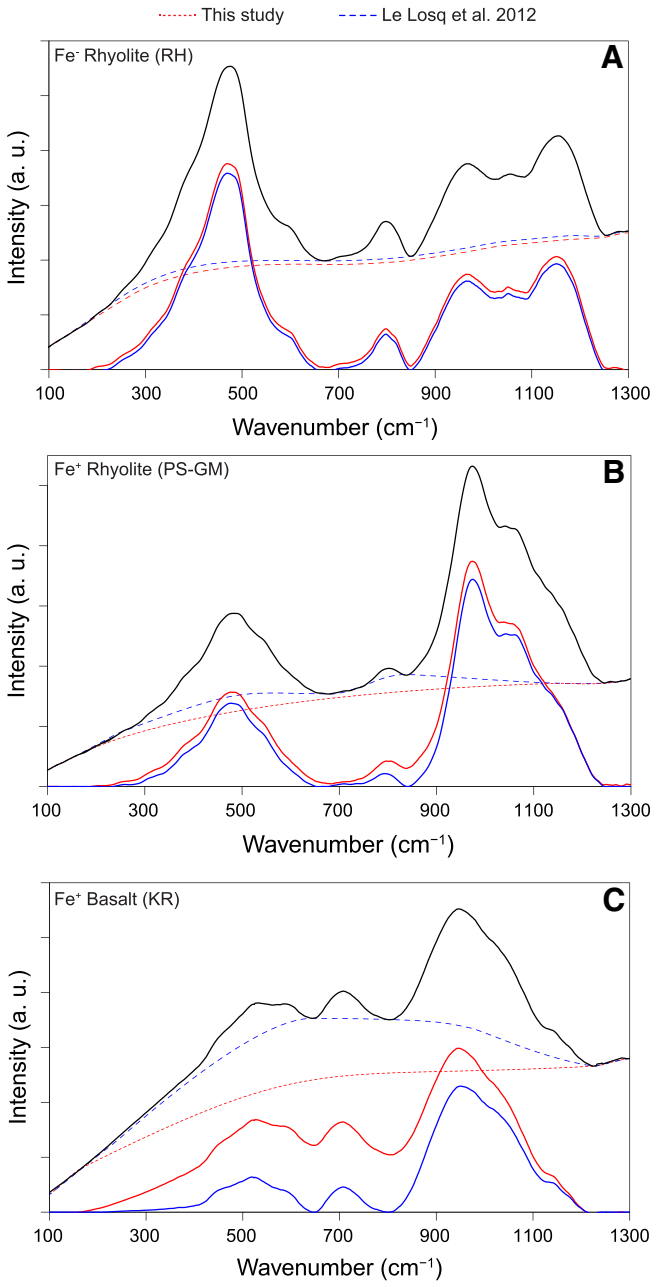

Fig. 6. Corrected Raman spectra of A) Fe^- rhyolite (RH3), B) Fe^+ rhyolite (PS-GM3) and C) Fe^+ basalt (KR2). Blue and red dashed lines represent the baseline according to the procedure reported in Le Losq et al. (2012) and this study, respectively. Baselines substantially diverge for SiO_2-poor samples resulting in a different LW band area. (For interpretation of the references to colour in this figure legend, the reader is referred to the web version of this article.)

Fig. 8 shows the calculated *A* coefficient (Eq. (1)) for each nanolite-free sample series starting from spectra acquired using the M spectrometer. Iron-poor glasses ($FeO_{tot.}$ < 4.5 wt%) exhibit a value slightly lower than the one provided by Le Losq et al. (2012). However, with increasing iron content, the coefficient increases up to $1.6 * \cdot 10^{-2}$ (iron-rich rhyolite PS-GM, $FeO_{tot.}$ = 9.55 wt%). We interpret the increase of *A* with iron content as the result of the effect of iron, and its oxidation state, on Raman spectra which is known to be particularly important in SiO_2-rich systems (Di Genova et al., 2016a).

Since the modulation of the baseline based on the SiO_2 content cannot remove completely the chemical dependence of the water estimation procedure, we adopted a single criterion for the baseline

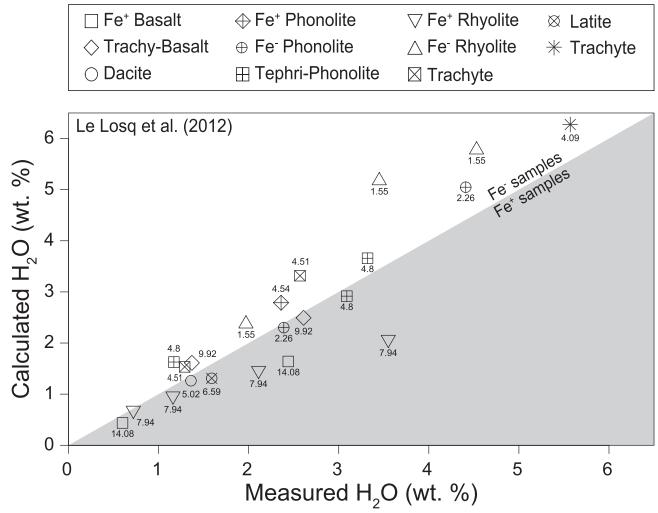

Fig. 7. Calculated (after Le Losq et al., 2012) versus measured water content. Numbers show the sample $FeO_{tot.}$ content in wt%. The model overestimates and underestimates the water content of iron-poor and iron-rich samples, respectively. All samples are nanolite-free.

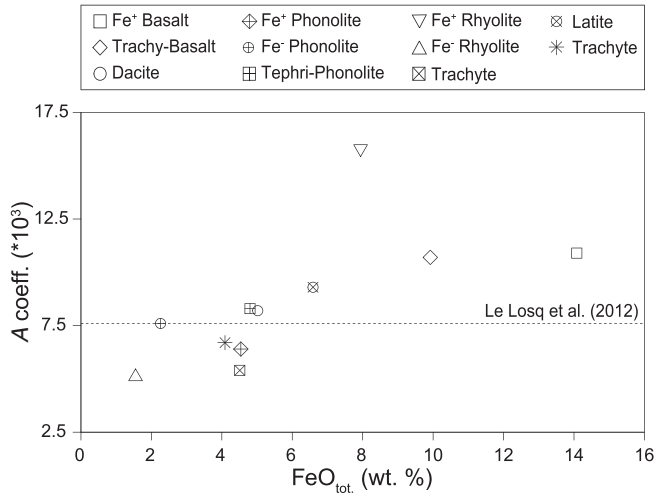

Fig. 8. Calculated *A* coefficient (Eq. (1)) as a function of the sample iron content. The dashed line represents the value provided by the authors ($7.609 * \cdot 10^{-3}$), considered independent of sample composition. Our results show that the coefficient increases with increasing iron content of the sample.

assessment regardless of the sample composition. A cubic spline was applied between 50–200 and 1240–1500 cm^{-1} for the LW region and between 2750–3100 and 3750–3900 cm^{-1} for the HW region. With this protocol, the nanolite-bearing glasses could be included in the analysis as the wavelength intervals chosen to assign the baseline in the LW region are not affected by their spectral contribution (Fig. 4A). Fig. 9A shows the water content as a function of the HW/LW area ratio using the M spectrometer. For each sample series, a linear relationship passing through the origin (Eq. (4)) was adopted for nanolite-free samples (green symbols, Fig. 9A):

$$H_2O\ (wt\%) = \frac{HW}{LW} \cdot m \tag{4}$$

where *m* is the linear fit coefficient (Table 2). Samples that experienced surface oxidation (Fig. 5A, B) during measurements using both spectrometers follow the observed relationship meaning that the internal calibration removes, or minimises, such an effect. Conversely, the nanolite-bearing samples (black symbols in Fig. 9A) deviate from linear trends. However, for the dacitic series (HO) we observed the lowest

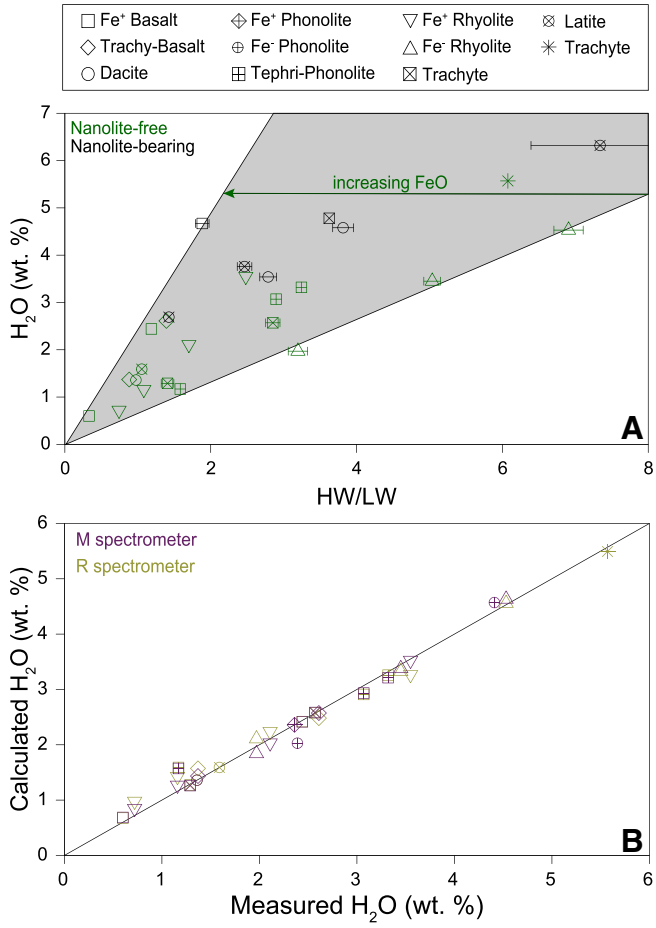

Fig. 9. A) Data from M spectrometer. Sample water content versus the HW/LW band area ratio calculated following the baseline protocol reported in this study. For each sample series, a linear relationship is observed when nanolite-free samples (green symbols) are considered. Nanolite-bearing samples (black symbols) do not follow such a trend. B) Data from both spectrometers. Comparison between measured and calculated water contents using Eq. (4) and data from Table 2. (For interpretation of the references to colour in this figure legend, the reader is referred to the web version of this article.)

deviation, while the latitic series highly deviates from the linearity. Therefore, these samples were excluded from the calculation of the fit coefficient (*m*, Eq. (4)). The sample water content was estimated using the Eq. (4) and parameters in Table 2 with a RMSE of 0.17 and 0.15 wt % for the M and R spectrometer, respectively (Fig. 9B).

The *m* coefficients reported in Table 2 can be used to retrieve the water content from Raman analyses whenever the chemical composition of the investigated sample is close to one of the samples used in this work.

We also investigated the possible chemical dependence of the fit parameter (*m*, Eq. (4)) in order to generalize our results. The Fig. 9A reveals that the fit parameter (*m*, Eq. (4)) shows a simple linear relationship with the iron content. A linear trend was observed for all the samples and both spectrometers (Fig. 10) suggesting that instrumental effects are removed (or minimised) with this procedure. We parameterised the iron dependence of the *m* parameter in Eq. (4) as it follows:

$$m = 0.096 * \mathrm{FeO} + 0.663 \tag{5}$$

where the FeO is the iron content in wt%. We estimated the water content of nanolite-free samples with a RMSE of 0.47 wt% for samples investigated with the M spectrometer and 0.29 wt% for the R spectrometer. This procedure is intended to be used when samples have different iron content from the standard and a different *m* coefficient is

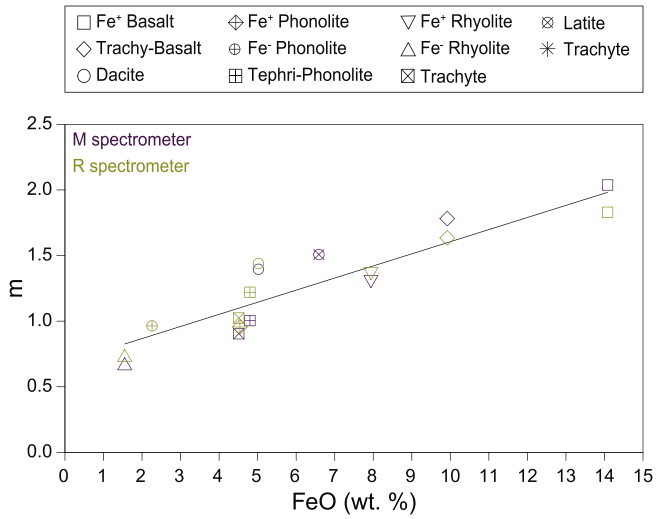

Fig. 10. Iron dependence of the *m* coefficient (Eq. (4)) for nanolite-free samples. For both spectrometers, a linear trend can be observed. Estimated water content using calculated *m* (Eq. (5)) and Eq. (4) are reported in Table 2.

expected. Moreover, in case the sample chemistry is unknown (i.e. small melt inclusions or in situ investigations), one may approximate the composition using the Raman spectrum (Di Genova et al., 2015, 2016b).

6. Conclusions

Here, we have shown how iron content, its oxidation state, and iron nanolites greatly affect Raman spectra of hydrous multicomponent glasses. Samples with composition spanning from basalt to rhyolite, including alkali- and iron-rich compositions, were used to explore and test procedures to estimate the water content of glasses through Raman spectroscopy. We recommend the following:

1) The sole water band area (HW, Fig. 5A, B) can be only used with nanolite-free samples regardless of the iron oxidation state of the glass. Sample and standard spectra must be acquired at the same depth (possibly at ~6 μm), instrumental conditions and using the same spectrometer. Sample oxidation during spectra acquisition can easily occur, especially when analysing iron- and alkali-rich samples. We found that 6 min of acquisition time and a laser power ~7 mW oxidised basaltic, dacitic, latitic, and iron-rich rhyolitic compositions, while ~5 mW are enough to alter alkali-rich (i.e. phonolite) sample. Increasing the acquisition time to ~26 min brings forth the oxidation for all samples excluding the calcalkaline rhyolite. Since the glass oxidation depends on the sample composition, acquisition time, and employed experimental settings (i.e. objective and laser power), we suggest repeating Raman measurements on the same spot and look at the evolution, if any, of the peak at ~970 cm^{-1} (Fe^{3+} band) which increases with increasing the Fe^{3+} content of the glass.
2) The water to silicate band ratio (HW/LW, Fig. 9A) linearly correlates with the water content of the glass. This procedure works when using nanolite-free samples and, importantly, is not affected by sample oxidation. Some nanolite-bearing samples (e.g. dacite) also follow a quasi linear trend. This procedure reduces instrumental effects. However, the slope (*m*, Eq. (4)) of the HW/LW ratio versus H_2O content depends on the iron content. For both spectrometers, we observed a linear relationship between the *m* coefficient and the iron content. Therefore, following the spectra treatment presented in this study, a unique calibration based on the iron content of the sample can be used to estimate the water content.

Acknowledgments

This study was supported by the NSFGEO-NERC "Quantifying disequilibrium processes in basaltic volcanism" (reference: NE/N018567/1). S. Sicola was supported by a MIUR fellowship to Roma Tre University PhD School. L. Spina wish to thank the ERC Consolidator "CHRONOS" project (reference: 612776). We thank M. Kaliwoda, R. Hochleitner, and A. Pisello for Raman measurements at the Mineralogical State Collection Munich (SNSB), L. Melekhova for some EMPA analyses in Bristol, S. Lo Mastro and D. De Felicis for SEM analysis at LIME laboratory (Roma Tre University), and R. Cioni for providing Vesuvius hydrated glass samples (79AD and 472AD). We also thank two anonymous reviewers for their contribution to the peer review of this work and helpful comments that helped us to improve this manuscript.

Appendix A. Supplementary data

Supplementary data to this article can be found online at https://doi.org/10.1016/j.chemgeo.2017.10.035.

References

Bachmann, O., Wallace, P.J., Bourquin, J., 2009. The melt inclusion record from the rhyolitic Kos Plateau Tuff (Aegean Arc). Contrib. Mineral. Petrol. 159, 187–202. http://dx.doi.org/10.1007/s00410-009-0423-4.

Behrens, H., Zhang, Y., 2009. H_2O diffusion in peralkaline to peraluminous rhyolitic melts. Contrib. Mineral. Petrol. 157, 765–780. http://dx.doi.org/10.1007/s00410-008-0363-4.

Behrens, H., Roux, J., Neuville, D.R., Siemann, M., 2006. Quantification of dissolved H_2O in silicate glasses using confocal microRaman spectroscopy. Chem. Geol. 229, 96–112. http://dx.doi.org/10.1016/j.chemgeo.2006.01.014.

Bell, R.J., Dean, P., 1972. The structure of vitreous silica: validity of the random network theory. Philos. Mag. 25, 1381–1398. http://dx.doi.org/10.1080/14786437208223861.

Bell, R.J., Bird, N.F., Dean, P., 1968. The vibrational spectra of vitreous silica, germania and beryllium fluoride. J. Phys. C Solid State Phys. http://dx.doi.org/10.1088/0022-3719/1/2/304.

Berry, A.J., Danyushevsky, L.V., O'Neill, H., Newville, M., Sutton, S.R., 2008. Oxidation state of iron in komatiitic melt inclusions indicates hot Archaean mantle. Nature 455, 960–963. http://dx.doi.org/10.1038/nature07377.

Blundy, J., Cashman, K.V., 2005. Rapid decompression-driven crystallization recorded by melt inclusions from Mount St. Helens volcano. Geology 33, 793. http://dx.doi.org/10.1130/G21668.1.

Bouhifd, M.A., Whittington, A.G., Richet, P., 2015. Densities and volumes of hydrous silicate melts: new measurements and predictions. Chem. Geol. 1–11. http://dx.doi.org/10.1016/j.chemgeo.2015.01.012.

Burgisser, A., Scaillet, B., 2007. Redox evolution of a degassing magma rising to the surface. Nature 445, 194–197.

Chabiron, A., Pironon, J., Massare, D., 2004. Characterization of water in synthetic rhyolitic glasses and natural melt inclusions by Raman spectroscopy. Contrib. Mineral. Petrol. 146, 485–492. http://dx.doi.org/10.1007/s00410-003-0510-x.

Di Genova, D., Romano, C., Hess, K.U., Vona, A., Poe, B.T., Giordano, D., Dingwell, D.B., Behrens, H., 2013. The rheology of peralkaline rhyolites from Pantelleria Island. J. Volcanol. Geotherm. Res. 249, 201–216.

Di Genova, D., Romano, C., Giordano, D., Alletti, M., 2014a. Heat capacity, configurational heat capacity and fragility of hydrous magmas. Geochim. Cosmochim. Acta 142, 314–333. http://dx.doi.org/10.1016/j.gca.2014.07.012.

Di Genova, D., Romano, C., Alletti, M., Misiti, V., Scarlato, P., 2014b. The effect of CO_2 and H_2O on Etna and Fondo Riccio (Phlegrean Fields) liquid viscosity, glass transition temperature and heat capacity. Chem. Geol. 377, 72–86. http://dx.doi.org/10.1016/j.chemgeo.2014.04.001.

Di Genova, D., Morgavi, D., Hess, K.U., Neuville, D.R., Borovkov, N., Perugini, D., Dingwell, D.B., 2015. Approximate chemical analysis of volcanic glasses using Raman spectroscopy. J. Raman Spectrosc. 46, 1235–1244. http://dx.doi.org/10.1002/jrs.4751.

Di Genova, D., Hess, K.U., Chevrel, M.O., Dingwell, D.B., 2016a. Models for the estimation of Fe^{3+}/Fe_{tot} ratio in terrestrial and extra- terrestrial alkali- and iron-rich silicate glasses using Raman spectroscopy. Am. Mineral. 101, 943–952.

Di Genova, D., Kolzenburg, S., Vona, A., Chevrel, M.O., Hess, K.U., Neuville, D.R., Ertelingrisch, W., Romano, C., Dingwell, D.B., 2016b. Raman spectra of Martian glass analogues: a tool to approximate their chemical composition. J. Geophys. Res. Planets 121, 740–752. https://doi.org/10.1002/2016JE005010.

Di Genova, D., Vasseur, J., Hess, K.U., Neuville, D.R., Dillon, R.T., 2017. Effect of oxygen fugacity on the glass transition, viscosity and structure of silica- and iron-rich magmatic melts. J. Non-Cryst. Solids 0–1. http://dx.doi.org/10.1016/j.jnoncrysol.2017.05.013.

Di Genova D., Kolzenburg S., Wiesmaier S., Dallanave E., Neuville D., Hess K.U., Dingwell D.B., in press, A chemical tipping point governing mobilization and eruption style of

rhyolitic magma. Nature, https://doi.org/10.1038/nature24488.
Di Muro, A., Giordano, D., Villemant, B., Montagnac, G., Scaillet, B., Romano, C., 2006a. Influence of composition and thermal history of volcanic glasses on water content as determined by micro-Raman spectrometry. Appl. Geochem. 21, 802–812. http://dx.doi.org/10.1016/j.apgeochem.2006.02.009.
Di Muro, A., Villemant, B., Montagnac, G., Scaillet, B., Reynard, B., 2006b. Quantification of water content and speciation in natural silicic glasses (phonolite, dacite, rhyolite) by confocal microRaman spectrometry. Geochim. Cosmochim. Acta 70, 2868–2884. http://dx.doi.org/10.1016/j.gca.2006.02.016.
Di Muro, A., Métrich, N., Mercier, M., Giordano, D., Massare, D., Montagnac, G., 2009. Micro-Raman determination of iron redox state in dry natural glasses: application to peralkaline rhyolites and basalts. Chem. Geol. 259, 78–88. http://dx.doi.org/10.1016/j.chemgeo.2008.08.013.
Dingwell, D.B., 2006. Transport properties of magmas: diffusion and rheology. Elements 2, 281–286. http://dx.doi.org/10.2113/gselements.2.5.281.
Dingwell, D.B., Romano, C., Hess, K.U., 1996. The effect of water on the viscosity of a haplogranitic melt under P-T-X conditions relevant to silicic volcanism. Contrib. Mineral. Petrol. 124, 19–28.
Fanara, S., Botcharnikov, R.E., Palladino, D.M., Adams, F., Buddensieck, J., Mulch, A., Behrens, H., 2015. Volatiles in magmas related to the Campanian Ignimbrite eruption: experiments vs. natural findings. Am. Mineral. 100, 2284–2297. http://dx.doi.org/10.2138/am-2015-5033.
Furukawa, T., Fox, K.E., White, W.B., 1981. Raman spectroscopic investigation of the structure of silicate glasses. III. Raman intensities and structural units in sodium silicate glasses. J. Chem. Phys. 75, 3226. http://dx.doi.org/10.1063/1.442472.
Galeener, F.L., 1982. Planar rings in vitreous silica. J. Non-Cryst. Solids 49, 53–62.
Gardner, J.E., Hilton, M., Carroll, M.R., 2000. Bubble growth in highly viscous silicate melts during continuous decompression from high pressure. Geochim. Cosmochim. Acta 64, 1473–1483.
Giordano, D., Nichols, A.R.L., Potuzak, M., Di Genova, D., Romano, C., Russell, J.K., 2015. Heat capacity of hydrous trachybasalt from Mt Etna: comparison with $CaAl_2Si_2O_8$ (An)–$CaMgSi_2O_6$ (Di) as basaltic proxy compositions. Contrib. Mineral. Petrol. 170, 48.
Gonnermann, H.M., Gardner, J.E., 2013. Homogeneous bubble nucleation in rhyolitic melt: experiments and nonclassical theory. Geochem. Geophys. Geosyst. 14, 4758–4773. http://dx.doi.org/10.1002/ggge.20281.
Hammer, J.E., Cashman, K.V., Voight, B., 2000. Magmatic processes revealed by textural and compositional trends in Merapi dome lavas. J. Volcanol. Geotherm. Res. 100, 165–192. http://dx.doi.org/10.1016/S0377-0273(00)00136-0.
Hartley, M.E., Maclennan, J., Edmonds, M., Thordarson, T., 2014. Reconstructing the deep CO_2 degassing behaviour of large basaltic fissure eruptions. Earth Planet. Sci. Lett. 393, 120–131. http://dx.doi.org/10.1016/j.epsl.2014.02.031.
Humphreys, M.C.S., Brooker, R.A., Fraser, D.G., Burgisser, A., Mangan, M.T., McCammon, C., 2015. Coupled interactions between volatile activity and Fe oxidation state during arc crustal processes. J. Petrol. 56, 795–814.
Kennedy, B., Spieler, O., Scheu, B., Kueppers, U., Taddeucci, J., Dingwell, D.B., 2005. Conduit implosion during Vulcanian eruptions. Geology 33, 581–584. http://dx.doi.org/10.1130/G21488.1.
Lange, R.A., Carmichael, I.S.E., 1987. Densities of Na_2O-K_2O-CaO-MgO-FeO-Fe_2O_3-Al_2O_3-TiO_2-SiO_2 liquids; new measurements and derived partial molar properties. Geochim. Cosmochim. Acta 2931–2946.
Lange, R.A., Carmichael, I.S.E., 1990. Thermodynamic properties of silicate liquids with emphasis on density, thermal expansion and compressibility. Rev. Mineral. Geochem. 24, 25–64.
Le Gall, N., Pichavant, M., 2016. Homogeneous bubble nucleation in H_2O- and H_2O-CO_2-bearing basaltic melts: results of high temperature decompression experiments. J. Volcanol. Geotherm. Res. 1–18. http://dx.doi.org/10.1016/j.jvolgeores.2016.10.004.
Le Losq, C., Neuville, D.R., Moretti, R., Roux, J., 2012. Determination of water content in silicate glasses using Raman spectrometry: implications for the study of explosive volcanism. Am. Mineral. 97, 779–790. http://dx.doi.org/10.2138/am.2012.3831.
Long, D.A., 1977. Raman Spectroscopy. vol. 2. McGraw-Hill, pp. 276.
Martel, C., Iacono-Marziano, G., 2015. Timescales of bubble coalescence, outgassing, and foam collapse in decompressed rhyolitic melts. Earth Planet. Sci. Lett. 412, 173–185. http://dx.doi.org/10.1016/j.epsl.2014.12.010.
McMillan, P.F., 1984. Structural studies of silicate glasses and melts-applications and limitations of Raman spectroscopy. Am. J. Sci. 69.
Mercier, M., Di Muro, A., Giordano, D., Métrich, N., Lesne, P., Pichavant, M., Scaillet, B., Clocchiatti, R., Montagnac, G., 2009. Influence of glass polymerisation and oxidation on micro-Raman water analysis in alumino-silicate glasses. Geochim. Cosmochim. Acta 73, 197–217. http://dx.doi.org/10.1016/j.gca.2008.09.030.
Métrich, N., Bertagnini, A., Di Muro, A., 2010. Conditions of magma storage, degassing and ascent at Stromboli: new insights into the volcano plumbing system with inferences on the eruptive dynamics. J. Petrol. 51, 603–626. http://dx.doi.org/10.1093/petrology/egp083.
Miyaji, N., Kan'no, A., Kanamaru, T., Mannen, K., 2011. High-resolution reconstruction of the Hoei eruption (AD 1707) of Fuji volcano, Japan. J. Volcanol. Geotherm. Res. 207, 113–129. http://dx.doi.org/10.1016/j.jvolgeores.2011.06.013.
Morizet, Y., Brooker, R.a., Iacono-Marziano, G., Kjarsgaard, B.a., 2013. Quantification of dissolved CO_2 in silicate glasses using micro-Raman spectroscopy. Am. Mineral. 98, 1788–1802. http://dx.doi.org/10.2138/am.2013.4516.
Mysen, B.O., 2003. Physics and chemistry of silicate glasses and melts. Eur. J. Mineral. 15, 781–802. http://dx.doi.org/10.1127/0935-1221/2003/0015-0781. (ST–Physics and chemistry of silicate gl).
Mysen, B.O., Virgo, D., Scarfe, C.M., 1980. Relations between anionic structure and viscosity of silicate melts - a Raman spectroscopic study. Am. Mineral. 65, 690–710.
Mysen, B.O., Virgo, D., Seifert, F.a., 1982. The structure of silicate melts: implications for chemical and physical properties of natural magma. Rev. Geophys. http://dx.doi.org/10.1029/RG020i003p00353.
Neuville, D.R., Mysen, B.O., 1996. Role of aluminium in the silicate network: in situ, high-temperature of glasses and melts on the join SiO_2-$NaAlO_2$. Geochim. Cosmochim. Acta 60, 1727–1737.
Ohlhorst, S., Behrens, H., Holtz, F., 2001. Compositional dependence of molar absorptivities of near-infrared OH- and H_2O bands in rhyolitic to basaltic glasses. Chem. Geol. 174, 5–20. http://dx.doi.org/10.1016/S0009-2541(00)00303-X.
Poe, B.T., Romano, C., Zotov, N., Cibin, G., Marcelli, A., 2001. Compression mechanisms in aluminosilicate melts: Raman and XANES spectroscopy of glasses quenched from pressures up to 10 GPa. Chem. Geol. 174, 21–31. http://dx.doi.org/10.1016/S0009-2541(00)00304-1.
Poe, B.T., Romano, C., Di Genova, D., Behrens, H., Scarlato, P., 2012. Mixed electrical conduction in a hydrous pantellerite glass. Chem. Geol. 320–321, 140–146. http://dx.doi.org/10.1016/j.chemgeo.2012.05.023.
Pouchou, J.-L., Pichoir, F., 1991. Quantitative analysis of homogeneous or stratified microvolumes applying the model “PAP”. In: Heinrich, K.F.J., Newbury, D. (Eds.), Electron Probe Quantitation. Springer, US, pp. 31–75. http://dx.doi.org/10.1007/978-1-4899-2617-34.
Romano, C., Giordano, D., Papale, P., Mincione, V., Dingwell, D.B., Rosi, M., 2003. The dry and hydrous viscosities of alkaline melts from Vesuvius and Phlegrean Fields. Chem. Geol. 202, 23–38. http://dx.doi.org/10.1016/s0009-2541(03)00208-0.
Scaillet, B., Macdonald, R., 2001. Phase relations of peralkaline silicic magmas and petrogenetic implications. J. Petrol. 42, 825–845.
Scaillet, B., Pichavant, M., 2004. Crystallization conditions of Vesuvius phonolites. In: Geophys. Res., (Abstract 6), pp. 3764.
Schmidt, B.C., Behrens, H., 2008. Water solubility in phonolite melts: influence of melt composition and temperature. Chem. Geol. 256, 258–267. http://dx.doi.org/10.1016/j.chemgeo.2008.06.043.
Seifert, F., Mysen, B.O., Virgo, D., 1982. Three-dimensional network structure of quenched melts (glass) in the systems SiO_2-$NaAlO_2$, SiO_2-$CaAl_2O_4$ and SiO_2-$MgAl_2O_4$. Am. Mineral. 67, 696–717.
Sharma, S.K., Mammone, J.F., Nicol, M.F., 1981. Raman investigation of ring configurations in vitreous silica. Nature. http://dx.doi.org/10.1038/292140a0.
Shishkina, T.A., Botcharnikov, R.E., Holtz, F., Almeev, R.R., Portnyagin, M.V., 2010. Solubility of H_2O- and CO_2-bearing fluids in tholeiitic basalts at pressures up to 500 MPa. Chem. Geol. 277, 115–125. http://dx.doi.org/10.1016/j.chemgeo.2010.07.014.
Stabile, P., Giuli, G., Cicconi, M.R., Paris, E., Trapananti, A., Behrens, H., 2017. The effect of oxygen fugacity and Na/(Na + K) ratio on iron speciation in pantelleritic glasses. J. Non-Cryst. Solids 0–1. http://dx.doi.org/10.1016/j.jnoncrysol.2017.09.051.
Stebbins, J.F., McMillan, P.F., Dillon, R.T., 1995. Structure, Dynamics, and Properties of Silicate Melts. Mineralogical Society of America, Chantilly.
Stolper, E.M., 1982. Water in silicate glasses: an infrared spectroscopic study. Contrib. Mineral. Petrol. 81, 1–17.
Thomas, R., 2000. Determination of water contents of granite melt inclusions by confocal laser Raman microprobe spectroscopy. Am. Mineral. 85, 868–872.
Thomas, S.M., Thomas, R., Davidson, P., Reichart, P., Koch-Müller, M., Dollinger, G., 2008. Application of Raman spectroscopy to quantify trace water concentrations in glasses and garnets. Am. Mineral. 93, 1550–1557. http://dx.doi.org/10.2138/am.2008.2834.
Tryggvason, E., 1986. Multiple magma reservoirs in a rift zone volcano: ground deformation and magma transport during the September 1984 eruption of Krafla, Iceland. J. Volcanol. Geotherm. Res. 28, 1–44. http://dx.doi.org/10.1016/0377-0273(86)90003-X.
Whittington, A., Richet, P., Holtz, F., 2000. Water and the viscosity of depolymerized aluminosilicate melts. Geochim. Cosmochim. Acta 64, 3725–3736.
Withers, A.C., Behrens, H., 1999. Temperature-induced changes in the NIR spectra of hydrous albitic and rhyolitic glasses between 300 and 100 K. Phys. Chem. Miner. 119–132.
Zajacz, Z., Halter, W., Malfait, W.J., Bachmann, O., Bodnar, R.J., Hirschmann, M.M., Mandeville, C.W., Morizet, Y., Müntener, O., Ulmer, P., Webster, J.D., 2005. A composition-independent quantitative determination of the water content in silicate glasses and silicate melt inclusions by confocal Raman spectroscopy. Contrib. Mineral. Petrol. 150, 631–642. http://dx.doi.org/10.1007/s00410-005-0040-9.
Zotov, N., Keppler, H., 1998. The influence of water on the structure of hydrous sodium tetrasilicate glasses. Am. Mineral. 83, 823–834.